Front. Phys. 13(1), 138203 (2018)
DOI 10.1007/s11467-017-0693-7

RESEARCH ARTICLE

High-temperature dynamic behavior in bulk liquid water: A molecular dynamics simulation study using the OPC and TIP4P-Ew potentials

Andrea Gabrieli, Marco Sant[1], Saeed Izadi[2], Parviz Seifpanahi Shabane[3], Alexey V. Onufriev[4,†], Giuseppe B. Suffritti[5,6,‡]

[1] *Dipartimento di Chimica e Farmacia, Università degli Studi di Sassari, Via Vienna 2, 07100 Sassari, Italy*
[2] *Department of Biomedical Engineering and Mechanics, Virginia Tech, Blacksburg, Virginia 24060, USA*
[3] *Department of Physics, Virginia Tech, Blacksburg, Virginia 24060, USA*
[4] *Departments of Computer Science and Physics, Virginia Tech, Blacksburg, Virginia 24060, USA*
[5] *Dipartimento di Chimica e Farmacia, Università degli Studi di Sassari, Via Vienna 2, 07100 Sassari, Italy*
[6] *Consorzio Interuniversitario Nazionale per la Scienza e Tecnologia dei Materiali (INSTM), Unità di ricerca di Sassari, Via Vienna 2, 07100 Sassari, Italy*
Corresponding authors. E-mail: [†] *alexey@cs.vt.edu,* [‡] *pino@uniss.it*
Received January 10, 2017; accepted May 2, 2017

Classical molecular dynamics simulations were performed to study the high-temperature (above 300 K) dynamic behavior of bulk water, specifically the behavior of the diffusion coefficient, hydrogen bond, and nearest-neighbor lifetimes. Two water potentials were compared: the recently proposed "globally optimal" point charge (OPC) model and the well-known TIP4P-Ew model. By considering the Arrhenius plots of the computed inverse diffusion coefficient and rotational relaxation constants, a crossover from Vogel–Fulcher–Tammann behavior to a linear trend with increasing temperature was detected at $T^* \approx 309$ and $T^* \approx 285$ K for the OPC and TIP4P-Ew models, respectively. Experimentally, the crossover point was previously observed at $T^* \approx 315 \pm 5$ K. We also verified that for the coefficient of thermal expansion $\alpha_P(T, P)$, the isobaric $\alpha_P(T)$ curves cross at about the same T^* as in the experiment. The lifetimes of water hydrogen bonds and of the nearest neighbors were evaluated and were found to cross near T^*, where the lifetimes are about 1 ps. For $T < T^*$, hydrogen bonds persist longer than nearest neighbors, suggesting that the hydrogen bonding network dominates the water structure at $T < T^*$, whereas for $T > T^*$, water behaves more like a simple liquid. The fact that T^* falls within the biologically relevant temperature range is a strong motivation for further analysis of the phenomenon and its possible consequences for biomolecular systems.

Keywords dynamic crossover, molecular dynamics, bulk liquid water, water models

PACS numbers 05.20.Jj, 05.10.-a, 05.90.+m

1 Introduction

The study of the multifarious properties of water — the most ubiquitous but also remarkably complex molecular liquid — is still a challenge for experimental, theoretical, and computational methods [1–3]. From a biological standpoint, the most interesting are arguably those properties and phenomena that manifest themselves in the physiological temperature range. Among the large number of water properties related to its dynamic heterogeneities and structural polymorphism [4], the existence of high-temperature dynamic phenomena was demonstrated on the basis of experimental data in bulk liquid water at $T^* \approx 315 \pm 5$ K [5–8].

It is well known that for many liquids, including water [9], self-diffusion exhibits Arrhenius behavior at $T > T^*$, whereas below some crossover temperature T^*, the behavior is super-Arrhenius [6, 8, 10]. Although for water

*Special Topic: Water and Water Systems (Eds. F. Mallamace, R. Car, and Limei Xu).

the change between these two distinct regimes is subtle and gradual, and the crossover point is thus difficult to pinpoint exactly [11], the crossover point clearly appears to occur at a physiologically relevant temperature ($T^* \approx 315 \pm 5$ K), which is potentially significant for biology.

Another experimental finding of potential biological relevance is the temperature variation of the compressibility and coefficient of thermal expansion in the physiologically relevant temperature range. Indeed, at $T^* \approx 315 \pm 5$ K, the isothermal compressibility $K_T(T,P)$ exhibits a minimum for all pressure values in the range $0.1 < P < 0.9$ GPa, whereas for the coefficient of thermal expansion $\alpha_P(T,P)$, all the isobaric $\alpha_P(T)$ curves cross at about the same T^* [6, 8]. As pointed out by Mallamace *et al.*, [8] experiments [12–20] show a "singular and universal expansivity point" at $T^* \approx 315$ K and $\alpha_P(T^*) \cong 0.44 \times 10^{-3}$ K^{-1}.

A further thermodynamic clue to the peculiar behavior of water in the physiologically relevant regime is a shallow minimum in the specific heat capacity at constant pressure C_P around 310 K [10, 21], and thus at a temperature close to T^*.

In addition, a *kinetic* argument can be made for a change in the Arrhenius plot of the dynamic quantities at some high temperature T^*. For supercooled and ambient-temperature water, the behavior of the dynamic quantities is super-Arrhenius [following the Vogel–Fulcher–Tammann (VFT) equation [22–24]] with the slope decreasing with increasing temperature. The slope of the Arrhenius plot of dynamic quantities, such as τ_2 and $1/D$, corresponds to the activation energy of the process, and the maximum of this slope for experimental measurements of D at the lowest available temperatures (about 240 K) [25] corresponds to about 60 kJ/mol, which is *larger* than the total cohesive energy of liquid water (about 42 kJ/mol). This high activation energy can be understood in terms of the concerted rotational–translational motion mechanism at the molecular level proposed by Laage [26–30]. Briefly, the mechanism involves rearrangement of a decreasing number of hydrogen bonds (HBs) with increasing temperature. As the temperature increases, the thermal energy reduces the heights of the energy barriers of the process; this reduction may involve a decrease in the number of HBs until a *minimum* number of relevant HBs is reached at some temperature T^*; consequently, the activation energy remains constant for $T > T^*$. Therefore, for $T > T^*$, the behavior of the dynamical quantities should become simple Arrhenius. It is worth mentioning that the concerted rotation–diffusion mechanism involves at least the first and second neighbor shells for a given water molecule; thus, if the minimum number of HBs involved in the process becomes small enough that it involves only the nearest-neighbor (NN) shell, the concerted mechanism should cease to operate, and the rotational and translational motions should at least partially decouple. In principle, T^* could occur at a temperature higher than the boiling point of water, but experimentally it was found at $T^* \approx 315 \pm 5$ K. The limiting activation energy fitted from the experimental data for the diffusion process is $E_a = 15.2 \pm 0.5$ kJ/mol [8], which is almost the same, within the statistical error, as the activation energy for rotational relaxation ($E_a = 16.5 \pm 0.6$ kJ/mol; see Section 3.1 below). Experimental support for the onset of structural changes in water at the molecular level at temperatures around T^* comes from a high-precision X-ray diffraction study of water in the range 254.2–369.5 K [31]. A detailed analysis of the diffraction data [32] showed that above the compressibility minimum (319 K, which coincides with T^* within the experimental error), the second maximum of the O–O radial distribution function (RDF) becomes less defined. This finding was interpreted by Schlesinger *et al.* [32] as the onset of collective tetrahedral fluctuations, which can be explained by a reduction in the HB network strength at $T > T^*$. Furthermore, behavior similar to the observed dynamic properties of bulk water at $T^* \approx 315 \pm 5$ K was also detected in the same temperature range in water confined in silica nanotubes (MCM-41) with diameter $d = 14$, 18, and 24 Å[8], and, more interestingly, in a single monolayer of water adsorbed on the globular protein lysozyme [8, 33]. On the basis of these observations, it was recently suggested [33] that the change in the dynamic behavior of water at T^* could be involved in, or exploited by, biochemical processes, because T^*, which corresponds to $\approx 42 \pm 5$°C, is close to the physiological temperature of many animals, in particular birds and mammals. The fact that the change occurs in a temperature range relevant for living organisms, which might have yet-undiscovered consequences, provides a strong motivation for further exploration of the phenomenon and other possible changes in water's structure and dynamics around T^*. Thus, atomistic simulations can help interpret existing experiments and provide guidance for future ones. In a recent simulation paper [34], the effect was detected computationally, most likely for the first time. That study, in addition to detecting the change in the Arrhenius plots of the rotational relaxation constant (τ_2) and of the inverse diffusion coefficient ($1/D$), considered the explicit trend of the distribution functions of the rotational relaxation constants, which shows a change from a narrow and regular distribution to a wider and asymmetrical one at a relatively high temperature. This trend could not be explained without invoking some change in the dynamical behavior of water. The analysis was completed by also considering the distribution of a *structural* quantity, namely, the tetra-

hedral order parameter, the trend of which shows some changes with changing T^*. The earlier study [34] employed two water models: the popular and well-known TIP4P-Ew [35] model and another one, which was developed for the study of water confined in nanoporous materials [36, 37], which in Ref. [34] was referred to as OP. However, the estimated values of T^* were 283 ± 2 and 276 ± 2 K for the TIP4P-Ew model and the OPC model, respectively, and deviated strongly from the experimental estimate of $\approx 315\pm5$ K [12–20]. The large deviation from the experimental T^* precludes reliable and quantitative analysis of the dynamical behavior of water at high temperature, especially in light of its possible relevance to biology: the nearly 40 K difference between the experimental and predicted values, while not as dramatic on the absolute temperature scale, may be critical from the biochemical perspective. Thus, it is not at all clear whether commonly used water models have the accuracy needed to describe this relatively subtle effect in quantitative agreement with experiment.

Motivated by the poor agreement with experiment of the T^* values estimated from simulations based on previously studied water models, here we use a recently developed water model referred to as the "optimal" point charge (OPC) water model [38] to study the high-temperature ($T > 300$ K) dynamic behavior in the liquid bulk. The OPC model is constructed using a completely different strategy from that of the mainstream water modeling parametrization techniques; the central idea of the OPC model is to search for a "global optimum" in the parameter subspace most relevant to the electrostatic properties of water molecules in the liquid phase so that the key experimental properties of bulk water at ambient temperature are best reproduced. The parametrization of the OPC model uses only a few key water properties at 298.16 K for fitting, yet the correct temperature dependence of most properties appears automatically over a wide range of temperatures [38], which motivated us to test the performance of the model by predicting the experimental value of T^*. To obtain a closer connection with experimental observables related to the dynamic behavior at T^*, here we also evaluate the coefficient of thermal expansion α_P and the HB and NN lifetimes. We compare the performance of the OPC water model with the predictions of the TIP4P-Ew model, one of the most commonly used water models of the same class.

2 Simulation details and models

The OPC water model was used to simulate the high-temperature dynamic behavior. The model was derived to optimally represent [39] the electrostatic charge distribution of the water model up to the octupole, with the C_{2v} symmetry being the only geometrical constraint. The geometry and parameters of the resulting four-point model are quite different from those of the TIP4P family [38]. Significant improvements in the accuracy of the bulk properties (average relative error of 0.76% for 11 key properties [38]) appear to give rise to improvements in practical biomolecular simulations [40–43]. Subtle microscopic properties such as the charge hydration asymmetry are also reproduced well by the OPC model [44].

For consistency with our previous work [34] with the TIP4P-Ew model, for the OPC model we used a cubic simulation box containing 343 water molecules. We employed the NAMD (Version 2.10) simulation package [45]. The investigated temperature range is from 180 to 340 K. First, we performed a 2 ns NPT run for each temperature at a fixed pressure of 1 bar (Langevin dynamics with Nosé-Hoover Langevin piston pressure control) to determine the mean lattice parameter (or the mean volume). Then we performed 1 ns NVT simulations to equilibrate the system at the desired temperature, keeping the volume fixed at the previously obtained value. Finally, we performed an NVE simulation for each temperature, where the duration was increased with decreasing temperature (ranging from a minimum of 5 ns to a maximum of 360 ns) to ensure convergence of the value of the rotational relaxation constant τ_2. Data were saved at regular intervals corresponding to 10^{-5} times the duration of the run $t_{\rm run}$. The particle mesh Ewald method for evaluating the Coulomb interactions was used; at the same time, a long-range correction to compensate for the truncated van der Waals interactions was applied.

To study the dynamics of water, we calculated the trends of the diffusion coefficients (D), rotational relaxation constants (τ_2), and mean lifetimes of the HBs and NNs of the molecules. In addition, we evaluated the coefficient of thermal expansion $\alpha_P(T,P)$ in a temperature range around the value of T^* for both models and for four pressures in the range $0.1 < P < 200$ MPa to verify whether all the isobaric $\alpha_P(T)$ curves crossed at T^*, as found experimentally [12–20]. The standard error of all the computed quantities was evaluated. The impact of this error on the results is discussed below. In particular, for the diffusion coefficient, it was recently pointed out [46] that the value of D obtained using the Ewald summations depends slightly on the simulation box size. However, as discussed in Ref. [34], the maximum error, which occurs at the highest temperature, is about twice the size of the symbols. Therefore, the dependence on the simulation box size does not substantially affect the results, as the corrections of the crossing temperatures are smaller than their error.

The rotational relaxation constant (τ_2), which is ac-

cessible by nuclear magnetic resonance and quasi-elastic neutron scattering experiments, was derived by computing the second-order rotational autocorrelation function [47] averaged over all the water molecules of the system:

$$C_2(t) = \frac{\langle P_2[\boldsymbol{u}(0)\cdot\boldsymbol{u}(t)]\rangle}{\langle P_2[\boldsymbol{u}(0)\cdot\boldsymbol{u}(0)]\rangle}, \quad (1)$$

where $\boldsymbol{u}(t)$ is the unit vector of the HOH plane, and P_2 is the second-order Legendre polynomial. The mean value of τ_2 was then computed by fitting $C_2(t)$ to the sum of two exponential decays and by choosing the *largest* relaxation time constant. The smaller time constant was on the order of a few picoseconds and can be interpreted as the relaxation time of the librational motion of the molecules [48–53]. Independently of the temperature or potential model, a good fit (values of the index $R^2 > 0.999$) was obtained by neglecting $C_2(t)$ for $C_2(t) < 2\times10^{-2}$. Indeed, for longer times, the correlation function became increasingly irregular, progressively departing from a double exponential form. For the OPC model, instead, a single exponential decay was sufficient to fit $C_2(t)$ very well, even for $2\times10^{-2} < C_2(t) < 0.3$. In Ref. [34], we also evaluated the distributions of the relaxation time constants among the molecules at different temperatures, which for the TIP4P-Ew potential model changed in width at $T \approx T^*$. In contrast to the case for the TIP4P-Ew model, for the OPC model these distributions did not show any noticeable change in the trend for $T > 230$ K and were not useful for evaluating T^*. Therefore, they are not considered in this paper.

Evaluation of the mean lifetime of the HBs from molecular dynamics (MD) simulations is a long-standing and controversial problem. After a long series of different contributions (for example, Refs. [54–57]), a critical review of the methods for deriving this quantity was published by Luzar [58], who discussed the two groups of methods previously proposed: *history-independent* methods based on specific time correlation functions and *history-dependent* methods based on averages taken over the duration of the HBs detected along the simulated trajectories. In a related paper [59], the discussion was extended to the dependence on the temperature. The problem was further considered in recent years [60–62], but no definitive assessment was made. In addition, the proposed experimental values [63–65] are model-dependent [66] and thus subject to uncertainty. To complicate the problem even further, the criteria that should be used to identify the HBs are still being debated [67–71]. Fortunately, as shown in Ref. [68], different criteria yield rather similar distributions of the number of HBs per molecule, so the discussion of the results should not be dramatically affected. We adopted the "geometrical" criteria [68], which are easier to apply in our simulations: $R_{OO} < R_{cut} =$ 3.3 Å and $\theta < \theta_{cut} = 30°$, where θ is the angle between the OH intramolecular bond and R_{OO}. We verified that changing the value of R_{cut} by some tenths of an Angstrom did not affect the results, so they should not be influenced by the small changes in the RDF vs. the temperature. Regardless of the criteria chosen to identify an HB, the most difficult point to address in evaluating the mean lifetime of HBs is intermittency. For a given molecule pair and for any given maximum value of R_{OO} or θ, it frequently happens that during the simulation, an HB seemingly disappears, but it is quickly re-formed, and this can be repeated a number of times until one of the molecules involved escapes from the NN shell and does not approach the previous one for a long time. This point does not affect the history-independent methods because the correlation functions are evaluated at the initial and final times without considering whether the HB was present at intermediate times. However, the evaluated mean lifetime is unambiguously defined only if the appropriate correlation function can be fitted with only one time constant, which rarely occurs, as we verified by performing test calculations.

Therefore, we preferred to use a history-dependent method with a procedure ensuring well-defined final values of the lifetimes. Indeed, history-dependent methods are statistically direct, but they must deal with intermittency [60–62]. If it is reasonable to consider an HB "alive" beyond short intermittencies, other criteria are needed to avoid extending its lifetime too much by including re-formation after a long detour. As suggested in Ref. [61], we chose to verify that, when the criteria defining the HB for a molecule pair are violated, the pair remains in the NN shell [the O–O distance remains smaller than $R_{shell}(OO)$, a distance corresponding to the first minimum in the O–O RDF]. For both models, we set $R_{shell}(OO)$ conservatively: $R_{shell}(OO) = 3.75$ Å. If this condition is fulfilled and the HB is re-formed, the HB is considered to be still "alive", and it is considered to be "dead" when the distance between the oxygens of the two molecules becomes larger than $R_{shell}(OO)$. In this case, the time spent to travel from a distance R_{OO} to a distance $R_{shell}(OO)$ is not included in the HB lifetime. This method leads to mean lifetimes that converge to definite values after a relatively small number of time steps, and we used it throughout. The algorithm used to evaluate the HB lifetime is shown in Fig. 1.

Note, finally, that at least for sufficiently high temperatures (outside of the deep supercooled regime), if two molecules form an HB involving a given hydrogen atom, the probability that the HB is broken and is re-formed between the same molecule pair involving the other hydrogen atom (HB switching) is very low, because this process has a relatively high energy barrier, whereas a concerted rotational–translational motion involving the

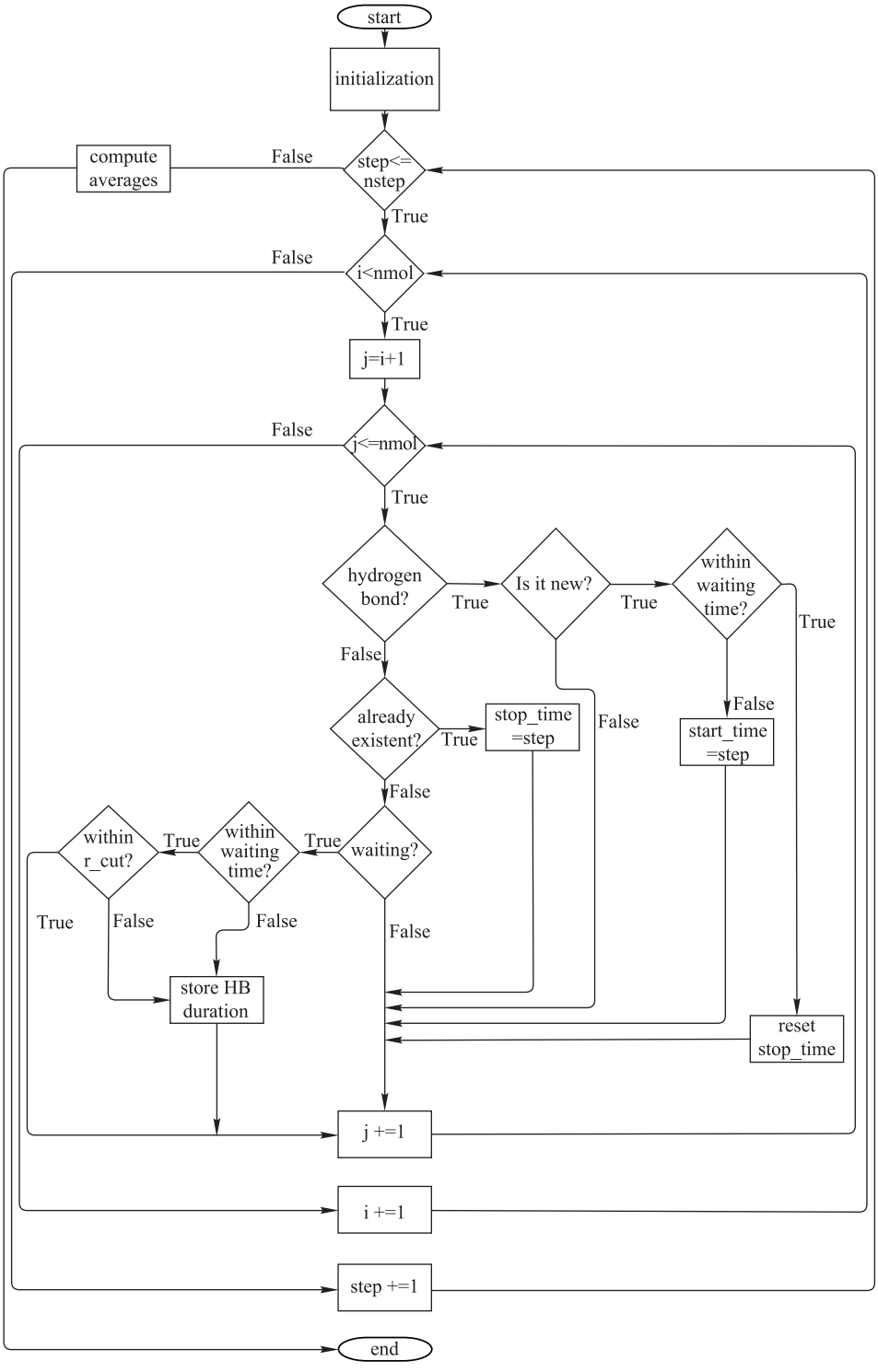

Fig. 1 Scheme of the HB lifetime evaluation algorithm. Here *nstep* is the number of trajectory frames stored, and *nmol* is the number of water molecules in the simulation (see text).

escape of one molecule from the NN shell is energetically favored and is the preferred route [26–30], as confirmed in a recent study using special cross-correlation functions [34]. Therefore, intermittency should not include significant HB switching, but we cautiously ensured that HB switching did not occur when the HB lifetimes were evaluated. The criteria used to define the NN lifetime (that is, the mean residence time of the water molecules in

the NN shell) become the same as those for the HB lifetimes by neglecting the constraint on θ. This ensures that the two lifetimes are directly comparable.

The thermal expansion coefficient was evaluated as

$$\alpha_P(T) = -\left(\frac{\partial \ln \rho(T)}{\partial T}\right)_P, \tag{2}$$

where $\rho(T)$ is the density as a function of temperature T at constant pressure P. The density was evaluated by a series of NPT simulations, and its logarithm was fitted using the formula $\ln \rho = a + \ln T + bT + cT^3$, where a, b, c are the free parameters of the fit. The expansion coefficient was then obtained from the temperature derivative of the fitting formula.

3 Results and discussion

3.1 Diffusion coefficients and rotational relaxation constants

Dynamic changes in liquids are usually studied by considering the slope and the functional dependence on the inverse temperature in the Arrhenius plots of some experimental or computed dynamical quantity, such as the diffusion coefficient D, or its inverse, and the rotational constant τ_2. In recent experimental studies of the behavior of water at high temperature, the experimental Arrhenius plot of D was considered [6–8, 11], and the temperature T^* at which the trend changes from super-Arrhenius (for $T < T^*$) to simple Arrhenius (for $T > T^*$) was detected. However, although experimental data are available in the appropriate temperature range [72–75], to the best of our knowledge a similar analysis of τ_2 was never conducted. This analysis is shown in Figure 2, where it appears that for three different experimental data sets, a clear change in the slope of the Arrhenius plots is visible at $T \approx 311$, 312, and 317 K for data sets (1) from Ref. [73], (2) from Ref. [74], and (3) from Ref. [75], respectively. The crossing temperature was estimated from the best fit of the piecewise function:

$$x(T) = \begin{cases} x_{\mathrm{A}} = \exp(E_{\mathrm{a}}/(k_{\mathrm{B}}T)), & T > T^*, \\ x_{\mathrm{VFT}} = \exp[E_{\mathrm{VFT}}/(k_{\mathrm{B}}(T - T_0))], & T \le T^*, \end{cases} \tag{3}$$

where $x = \tau_2$ (or $x = 1/D$ in the following when appropriate); the subscripts A and VFT represent the Arrhenius equation and VFT equation [22–24], respectively; E_{a} is the Arrhenius activation energy; k_{B} is the Boltzmann constant; E_{VFT} is a parameter with dimensions of energy; and T_0 is a parameter with dimensions of temperature. In a semilogarithmic plot of x vs. $1/T$, the Arrhenius plot is linear, whereas the plot of the VFT equation is curvilinear, where the slope vs. $1/T$ increases. The resulting mean value of the experimental crossover temperature for τ_2 is $T^* \approx 313 \pm 5$ K, which is within the range derived from the trends of D and the expansion coefficients [6–8]. Above T^*, the weighted mean of the experimental Arrhenius activation energy is $E_{\mathrm{a}} = 16.5 \pm 0.6$ kJ/mol, which is almost the same, considering the statistical error, as the Arrhenius activation energy for the self-diffusion coefficient, $E_{\mathrm{a}} = 15.2 \pm 0.5$ kJ/mol. One can debate whether the above interpretation is the only one possible; indeed, a power law fitting was used, at least for D, in a number of experimental papers, although no physical rationale for the procedure was given. However, the good correspondence with the trend of the diffusion coefficient and the accurate fit to the data make it at least plausible.

Figure 3 compares the experimental values with the simulations results obtained for the OPC and TIP4P-Ew models. As shown in Ref. [38] for the OPC model and in Ref. [34] for the TIP4P-Ew model, the computed diffusion coefficients agree well with the experimental data, and they are not reported here. For both potentials, a

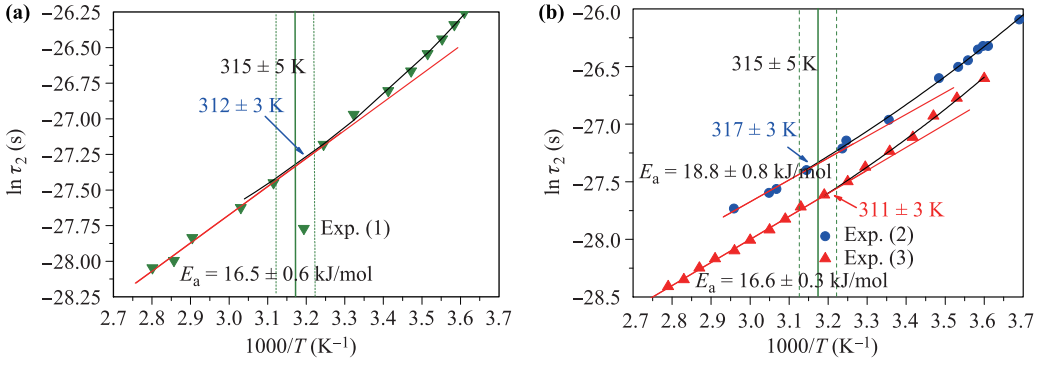

Fig. 2 Arrhenius plot of the rotational relaxation constants τ_2 for three sets of experimental values: **(a)** (1) from Ref. [73], **(b)** (2) from Ref. [74] and (3) from Ref. [75]. Solid lines are least-square fits to the Arrhenius equation for high temperatures (*red*) and to the VFT equation [22–24] in the low-temperature range (*black*). For clarity, both lines are extended beyond the crossover point.

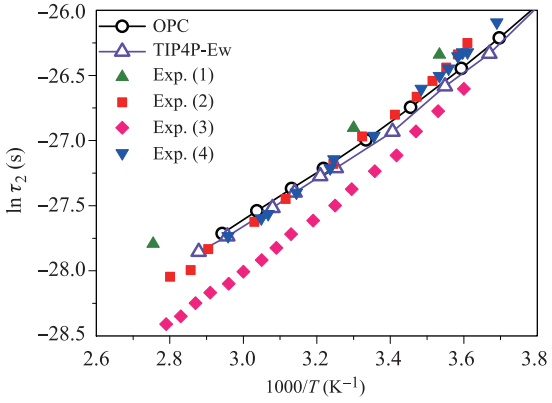

Fig. 3 Arrhenius plot of the mean rotational relaxation constants compared with three sets of experimental results for the OPC (open circles) and TIP4P-Ew (open triangles) models. Experimental values from (1) Ref. [72], (2) Ref. [73], (3) Ref. [74], and (4) Ref. [75]. The lines are guides for the eye.

dynamic crossover was detected in the computed Arrhenius plots of τ_2 and $1/D$ as the transition from a VFT equation [22–24] fit at lower temperatures (characteristic of a fragile liquid) and an Arrhenius fit at higher temperatures (characteristic of a normal liquid). The VFT-to-normal-Arrhenius change, which was found experimentally at $T^* \approx 315 \pm 5$ K (see the Introduction), can be detected in our simulations results in the Arrhenius plot of τ_2 at $T^* \approx 308 \pm 5$ K and $T^* \approx 285 \pm 5$ K for the OPC and TIP4P-Ew models, respectively [see Figs. 4(a) and (c)]. Similar results are obtained from the Arrhenius plots of $1/D$ [Figs. 4(b) and (d)], for which the resulting crossover temperatures are $T^* \approx 309 \pm 5$ K and $T^* \approx 285 \pm 5$ K for the OPC and TIP4P-Ew models, respectively. Therefore, the estimate of T^* given by the OPC model is gratifyingly good.

We investigated the robustness of the value of T^* (obtained from the inverse diffusion coefficient $(1/D)$) to the details of the simulation protocol. For the test, we employed an alternative, considerably more expensive but arguably more accurate [35, 38], protocol for the calculation of the water self-diffusion coefficient; the protocol was used previously to parameterize the OPC and TIP4P-Ew water models. Briefly, instead of performing a single long *NVE* simulation (>5 ns), the self-diffusion was computed from 80 intervals of *NVE* (20 ps) and *NPT* (5 ps) (see Ref. [38]). The resulting T^* value was estimated to be 308.5 ± 5 K, which is consistent with the value of 309 ± 5 K shown in Fig. 4(b). We note in passing that the computed values of the activation energy for the rotational relaxation ($E_a = 14.6 \pm 0.6$ kJ/mol and $E_a = 15.5 \pm 0.4$ kJ/mol for the OPC and TIP4P-Ew potentials, respectively) are in good agreement with the value of $E_a = 16.5 \pm 0.6$ kJ/mol estimated from the experimental data (see above). The small differences between the values of T^* obtained from the fits of different quantities may result from the fitting procedure. On the other hand, the temperature was sampled at intervals of about 10 K, so differences of a few degrees in the crossover temperature are not unexpected. In addition, the errors in the calculated quantities, which were evaluated by running independent simulations at the same temperature, for three different constant temperatures, are at most on the order of 1%, or, on the logarithmic scale, the same size as the symbols used in Figure 4. In conclusion, a conservative overall statistical error of 5 K is assigned throughout to the estimates of the crossing temperatures derived from the reported simulation results.

The temperature range of the plots in Figure 4 is restricted to values suitable for locating the crossover at T^*, but we extended the simulations for both models in the supercooled regime down to about 180 K, and we detected the low-temperature fragile–normal dynamic crossover at $T_L \approx 222 \pm 5$ K (see the Appendix) and $T_L \approx$ 200–203 K [34] for the OPC and TIP4P-Ew models, respectively. It is well known that the crossover temperature T_L cannot be observed directly by experiment because the crossover occurs under deep supercooling conditions, where the freezing temperature may be shifted only by using special techniques such as ultrafast cooling and measurements [76]. However, by extrapolating the available experimental data points, T_L was estimated to be about 225 K [10, 77–79]. The corresponding value obtained from the OPC model is very close to this estimate, and the OPC model outperforms the TIP4P-Ew model overall in estimating the dynamic crossover temperatures. More details about the simulations over the low-temperature range are reported in the Appendix.

We note that the fittings of the Arrhenius plots of τ_2 and $1/D$ alone are not sufficient for accurate evaluation of the temperature T^* owing to the sensitivity of the measured or calculated crossover point to data uncertainties. However, the specific value of T^* is further supported by an analysis of the coefficients of thermal expansion and of the HB and NN lifetimes and, at least for the TIP4P model, by further analyses reported in a previous paper [34]. The crossing temperatures in Figure 4 could depend on the choice of points to be fitted, in which case the temperature values are subject to an uncertainty of a few Kelvins. In fact, the reported experimental values of T^* have error margins of a few Kelvins; considering the trend of different sets of experimental values of τ_2 in Fig. 2, the estimated error in the value of T^* is about 5 K.

3.2 Coefficient of thermal expansion

We studied the coefficient of thermal expansion for comparison with the results that Mallamace *et al.* [6] re-

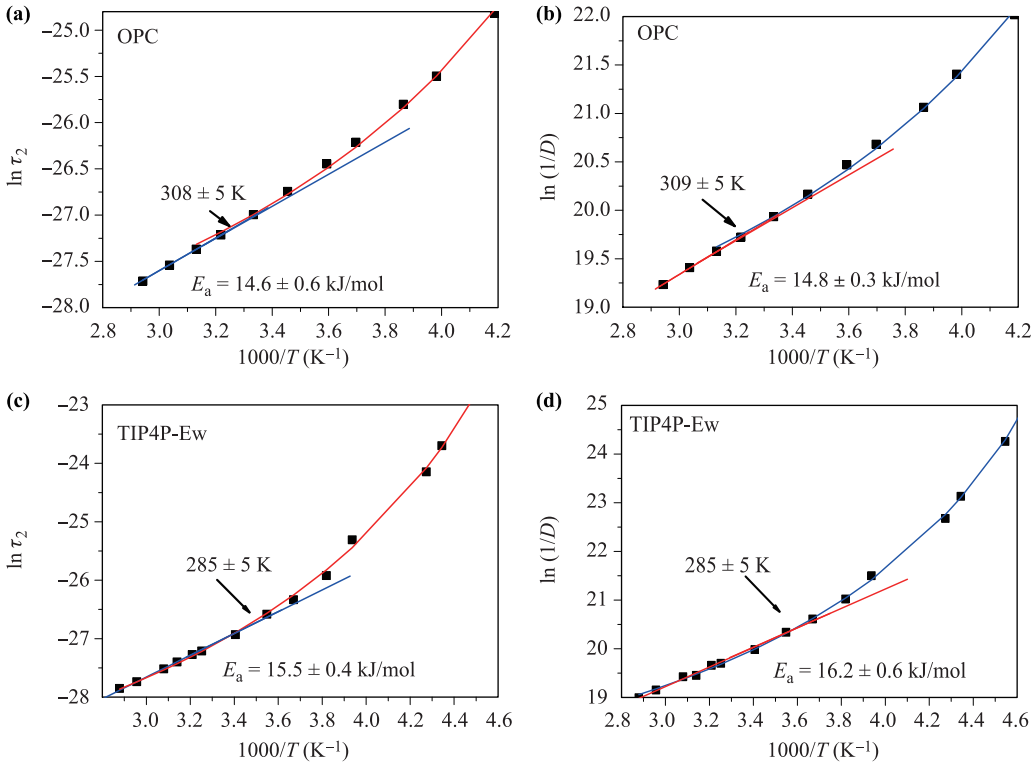

Fig. 4 Arrhenius plots of the computed rotational relaxation constants τ_2 for the **(a)** OPC and **(c)** TIP4P-Ew models, as well as of the computed inverse diffusion coefficients $1/D$ for the **(b)** OPC and **(d)** TIP4P-Ew models. The lines are fits to the Arrhenius equation (on the left, higher temperatures) and the VFT equation [22–24] (on the right, lower temperatures). The arrows show the crossover temperature.

ported in their Fig. 3. In particular, we computed the thermal expansion coefficient [see Eq. (2)] as a function of T at various pressures. The curves for the various pressures should cross at a fixed "universal" temperature. In our 2 ns NPT simulations using the OPC model, this is true for pressures up to 200 MPa and occurs at a temperature $T^* \approx 323 \pm 5$ K, which is close to the experimental value, $T^* \approx 315 \pm 5$ K. Interestingly, the value of the thermal expansion coefficient at this temperature is very close to the experimental value ($\alpha_P \approx 0.46 \times 10^{-3}$ K^{-1} vs. $\alpha_P \approx 0.44 \times 10^{-3}$ K^{-1} from experiments [12–20]). The value obtained from the TIP4P-Ew model is $\alpha_P \approx 0.38 \times 10^{-3}$ K^{-1} at a temperature $T^* \approx 304 \pm 5$ K. For the TIP4P-Ew model, the value of $\alpha_P(T^*)$ is slightly lower than the experimental one but is still in reasonably good agreement. However, when we consider the coefficient of thermal expansion, although for α_P the computed values of the crossing temperatures are, at least for the OPC model, in agreement with the experiment, for both models they are higher (by about 15–20 K) than the values of T^* estimated using the Arrhenius plots of the simulated τ_2 and $1/D$, as well from the crossing of the lifetimes of the NNs and HBs (see below), which are all within a few Kelvins. On the other hand, α_P is a property of the bulk, and its connections with the molecular dynamic properties are not straightforward; a deeper discussion is needed, in our opinion, to unravel this discrepancy.

In addition, for pressures higher than those reported in Fig. 5, the crossing is no longer observed at the same temperature, but at a higher T. From the data in Fig. 5, it is possible to derive the temperatures of maximum density of the two water models, which correspond to the temperatures at which the expansion coefficient α_P is zero at 0.1 MPa. Their values agree with those reported in Refs. [35] and [38], which are 274 and 272 ± 1 K for the TIP4P-Ew and OPC models, respectively, vs. the experimental value of 277 K.

3.3 Mean lifetimes of HBs and NN molecules

Finally, we evaluated the mean lifetimes of the NNs in the first shell around a molecule and of the HBs formed by a molecule. Interestingly, they cross at approximately T^* (see Fig. 6). Moreover, at the same temperature, the trend clearly changes. In particular, for the OPC model, the crossing T is practically the same as that obtained from the Arrhenius plots of τ_2 and $1/D$, whereas for the

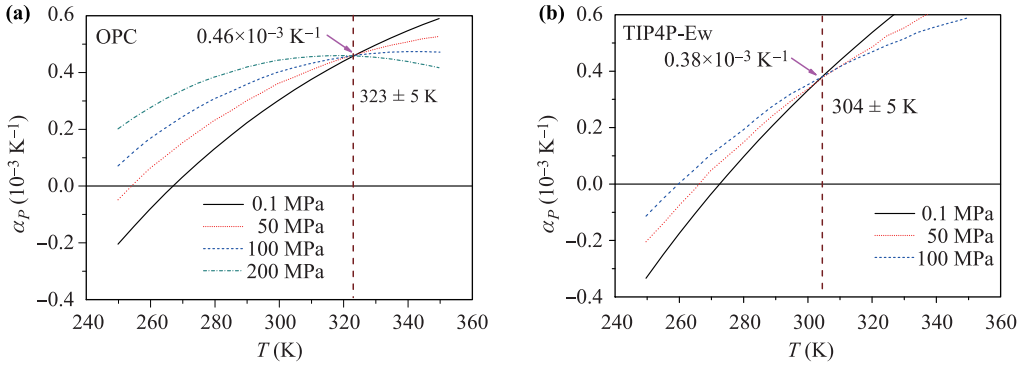

Fig. 5 Expansion coefficients vs. T at different pressures, evaluated from simulations for the **(a)** OPC and **(b)** TIP4P-Ew models.

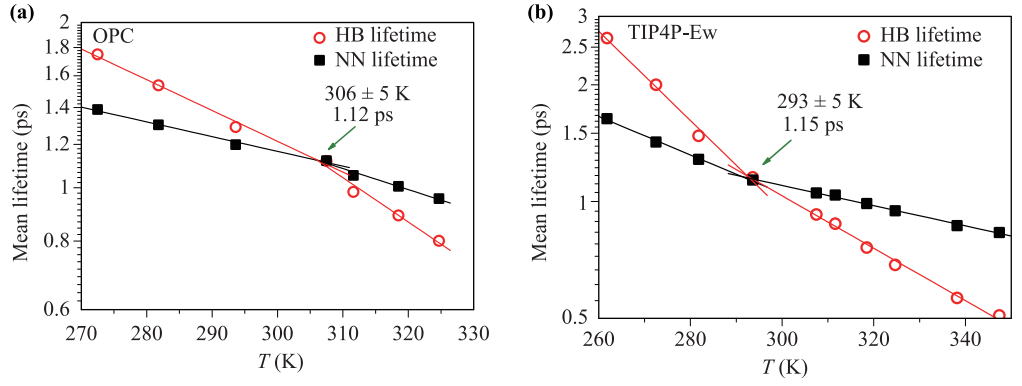

Fig. 6 Mean lifetimes of the NNs and of the HBs formed by a molecule in the **(a)** OPC and **(b)** TIP4P-Ew models. The lines are linear fittings of the computed data.

TIP4P-Ew model, it is slightly higher ($\approx 293 \pm 5$ K vs. $\approx 285 \pm 5$ K). The crossing of the NN and HB lifetimes means that for $T > T^*$, the HB lifetime is longer than the time that the molecules remain within the NN shell. For $T < T^*$, the HB lifetime is longer than the time that the molecules remain in the NN shell, as they are engaged in the concerted rotational–translational motion mechanism proposed by Laage [26–30] involving the rearrangement of a number of HBs *beyond* the NN shell (see also the Introduction). With increasing T, the process may involve a decrease in the number of HBs until a minimum number of HBs is reached at some temperature T^*. This minimum will occur when the HB lifetime becomes so short that the HBs break, on average, *before the associated diffusion jump is completed*, and thus the associated time-scale is shorter than the lifetime of the molecules in the NN shell. Therefore, *the minimum number of HBs involved in the process is just the number of HBs formed within the first NN shell*. Consequently, the rotational and translational motions become at least partially decoupled, and diffusion can occur by direct translation of an NN molecule (no longer involved in an HB after the quick breaking of the incipient correlated process) to the next NN shell, as in simple liquids. This picture is in line with the above interpretation of the trend of the second-shell peak of the O–O RDF at temperatures above the compressibility minimum (319 K), as derived in a recent X-ray diffraction experiment [31]. Schlesinger *et al.* [32] interpret this trend as the onset of collective fluctuations of the tetrahedral local structure of water. Indeed, our simulations show that the importance of H bonding is reduced and fewer HBs are present as the temperature is increased [see Fig. 7 and Fig. 14(c) of Ref. [34]]. Therefore, for $T < T^*$, the HB network is dominant, and for $T > T^*$, a simple liquid-like behavior sets in, as suggested by experimentalists [33], and, in addition, the simulated HB and NN lifetimes at T^* correspond to the expected experimental lifetime of about 1 ps. Interestingly, the same characteristic lifetime was reported in a recent study [80], which showed that, under a suitable averaging of the intermolecular potential and using the principle of the corresponding thermodynamic states, the behavior of many thermodynamic properties of water, such as the specific volume, heat of evaporation, shear viscosity, and triple point, is similar to that of these properties of argon, especially at temperatures

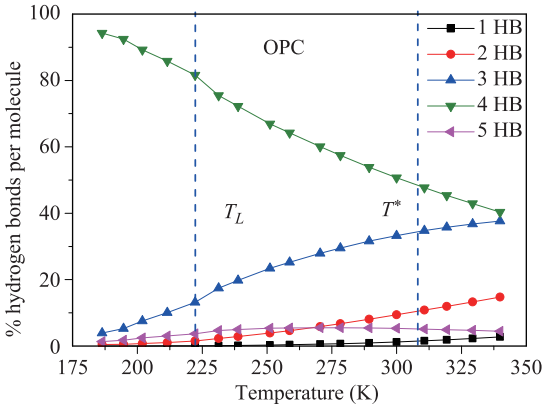

Fig. 7 Distributions of the number of HBs per molecule for the OPC model. The vertical dashed lines show the average values of T_L and T^*. The lines are guides for the eye.

of $315 < T < 550$ K. In contrast, at "$T < 315$ K, i.e. in the supercooled and normal states adjacent to the melting point, the properties of water are determined by the [H-bonded] clusters, [in] which lifetime τ_c becomes essentially greater than the characteristic time $\tau_s \approx 10^{-12}$ s for the thermal motion of molecules [81]."

4 Conclusions

In this study, we performed classical MD simulations to investigate the molecular-level mechanism of the high-temperature change in the dynamic behavior of liquid bulk water found experimentally at $T^* \approx 315 \pm 5$ K. Two water models were employed: the recently proposed "globally optimal" point charge (OPC) model and, for comparison, the well-known TIP4P-Ew model. By considering the Arrhenius plots of the rotational relaxation constants and inverse diffusion coefficients, the change in the Arrhenius plot was detected at $T^* \approx 309 \pm 5$ K and $T^* \approx 285 \pm 5$ K for the OPC and TIP4P-Ew models, respectively.

The presence of a dynamic change in the simulations was confirmed by evaluating the mean lifetimes of the NNs around a molecule and the HBs formed by a molecule, which were found to cross at approximately T^*, and independently by verifying that for the coefficient of thermal expansion $\alpha_P(T, P)$, all the isobaric $\alpha_P(T)$ curves cross at approximately T^*, as found experimentally [12–20].

As for the crossing of the mean lifetimes of the NNs and HBs, the corresponding molecular-level mechanism seems to be related to a relaxation of the HB network of bulk water, which is apparently connected to the shortening of the HB lifetimes below the residence time of the molecules in the NN shell, which allows the molecules to become "free", approaching the behavior of a simple liquid, as proposed by experimentalists [33], at the expected lifetime of about 1 ps. As mentioned above, this conclusion is also supported by thermodynamic considerations derived from the experimental phase diagram of water [80, 81]. It appears that this feature is shared by water simulated using different models.

We believe that this work, in addition to faithfully reproducing the experimental data, especially for the OPC model, provides new physical insight. The crossing of the HB and NN lifetimes shown in Fig. 6 entails, in our opinion, a subtle but meaningful change in the diffusion mechanism of bulk water at approximately T^*. As discussed in the previous section, for $T < T^*$, the persistence of HBs for times longer than the residence times of the molecules in the NN shell is associated with an apparent concerted translational–rotational diffusion mechanism. For $T > T^*$, in contrast, the HBs break on average before the concerted mechanism occurs; thus, diffusion more likely occurs by direct translation of an NN molecule to a next NN shell, as in simple liquids.

Last, but certainly not least, it is the very subtlety of the dynamics of water at high temperature that is advantageous for testing newer water models in search of those that may faithfully reproduce water properties across a range of temperatures.

Indeed, a wide class of biomolecular properties is very sensitive to the details of water models, and we outline the need for water models to reproduce subtle water properties correctly in order to obtain predictive power in estimates of protein–ligand binding and protein folding energetics. For example, it was shown recently that the protein–ligand binding energy depends strongly on the water model used, where the size of the dependence is comparable to the binding energy itself [82] (see also Ref. [41]). A similar sensitivity is observed for the protein folding free energy [83–86].

Overall, one can conclude that to completely understand the properties of water at the molecular level, many different statistical tools related to both the dynamical and structural quantities should be used, and those proposed in this study were demonstrated to be useful. Work is in progress to extend this study to water adsorbed on the surface of biological molecules and in microporous materials. In general, computer simulations are often employed to support both experimental and theoretical work by providing suggestions regarding the behavior of water at the atomic level [26–30, 61, 62, 87–92]; in many cases, the unsurpassed spatial and temporal resolution of these simulations is indispensable for elucidating subtle issues such those related to the lifetime of HBs [58]. Therefore, the accuracy of the employed water models is critical. The noteworthy performance of the recently proposed OPC model in reproducing the

experimental features of the high-temperature dynamic crossover in bulk water suggests that it would be useful to explore further bulk properties of OPC water, especially with respect to subtle effects such as the dynamic crossover. It may also be interesting to explore the model's accuracy in simulating the complete phase diagram of water. Because the OPC model is a rigid, non-polarizable water model, one can expect larger deviations from experiment outside of the liquid phase for which the model was originally designed. Still, these deviations might turn out to be smaller than those of other water models with the same level of simplicity and efficiency.

Acknowledgements This research was supported by the Italian Ministero dell'Istruzione, dell'Università, e della Ricerca (MIUR), by Regione Autonoma della Sardegna (Italy), by Università degli studi di Sassari, and by Istituto Nazionale per la Scienza e Tecnologia dei Materiali (INSTM), which we acknowledge. The "Consorzio COSMOLAB" is also acknowledged for the resources provided within the CyberSar Project. A.V.O. acknowledges support from the US National Institutes of Health (NIH GM076121). We are grateful to Professor G. Franzese for useful discussion of our results and for encouragement in continuing our study. Professor F. Mallamace is gratefully acknowledged for critically reading the manuscript and making useful suggestions.

Appendix A Low-temperature results for the OPC model

As for the simulations using the TIP4P-Ew potential, for which the results are reported in Ref. [34], those using the OPC model were performed over the temperature range 180–340 K at intervals of 10 K. In both cases, we used a protocol ensuring good equilibration even at low temperature, because in the supercooled regime, molecular motion slows dramatically, and special care is required [93]. The simulations were started at the highest temperature (340 K), and the system was cooled stepwise in 10 K increments starting from the final phase space configuration of the preceding temperature. For each temperature, a 2 ns NPT simulation was performed using the procedure implemented in the NAMD package at a fixed pressure of 1 bar (Langevin dynamics with Nosé-Hoover Langevin piston pressure control). Then we performed 1 ns NVT simulations to equilibrate the system at the desired temperature, keeping the volume fixed at the previously obtained value. Finally, the resulting MD simulation box side was fixed, and an NVE simulation was run, where the duration was increased with decreasing temperature to ensure the convergence of the value of the rotational relaxation constant τ_2. For the OPC model, the duration of the simulations ranged from 2 ns at 340 K to 360.5 ns at 180 K. Therefore, at each cooling step, the system started from a configuration accurately equilibrated at a slightly higher temperature. This protocol should ensure good equilibration even at the lowest temperatures, and indeed the computed quantities show a smooth trend, as expected. The value of the temperature dynamic crossover in the supercooled regime T_L was obtained from the Arrhenius plots of the inverse diffusion coefficient and rotational relaxation constant τ_2. These plots are shown in Fig. A1.

The crossing temperature was estimated from the best fit of the piecewise function given by Eq. (3); for both dynamical quantities, $1/D$ and τ_2, we obtained $T_L = 222 \pm 5$ K, which is very close to the value extrapolated from experimental data (approximately 225 K [10, 77–79]). We note that the activation energies for $T < T_L$ ($E_a = 51.9 \pm 1.8$ and $E_a = 54 \pm 3$ kJ/mol for τ_2 and D, respectively) are noticeably higher than those obtained when the TIP4P-Ew potential is used, which are $E_a = 11 \pm 4$ and $E_a = 30.2 \pm 0.6$ kJ/mol for D and τ_2, respectively, indicating that the motion of water molecules in this regime is much slower for the OPC model than

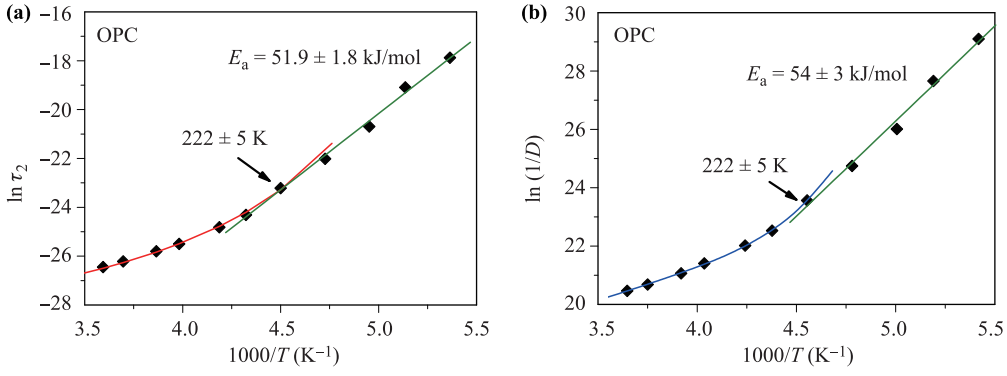

Fig. A1 Arrhenius plots for the OPC model of the **(a)** computed rotational relaxation constants τ_2 and **(b)** computed inverse diffusion coefficients $1/D$. The lines are the fit to the VFT equation [22–24] (on the left, higher temperatures) and to the Arrhenius equation (on the right, lower temperatures). The arrows show the crossover temperature.

for the TIP4P-Ew model.

An experimental estimation of the diffusion coefficient in supercooled water from 126 to 262 K was given in a recent paper [94]. Using a pulsed-laser heating technique, the growth rate of crystalline ice from amorphous solid water was measured, and the self-diffusion coefficient $D(T)$ was estimated from the Wilson–Frenkel model of crystal growth [95]. From this estimate of $D(T)$, a value of $T_L \approx 228$ K was found, in agreement with the previous extrapolated value and with that obtained from our simulations using the OPC model, $T_L = 222 \pm 5$ K. For $T < T_L$ the trend of the experimental estimate of $D(T)$ is Arrhenius, as expected, with an activation energy $E_a \approx 76$ kJ/mol, which is higher than, but still of the same order as, the value obtained using the OPC model, $E_a = 54 \pm 3$ kJ/mol. This is in contrast to the result for the TIP4P-Ew model, for which the disagreement is nearly 700%.

Finally, we remark that the values of T_L and E_a for two other water models of the TIP4P family, namely, the original TIP4P model [96] and the more recent TIP4P/2005 model [97], are $T_L \approx 210$ K, $E_a = 42.1$ kJ/mol and $T_L \approx 206$ K, $E_a = 45.3$ kJ/mol, respectively [98]. In conclusion, the agreement of the values of T_L and E_a with the most recent experimental estimates are in favor of the OPC model.

References

1. P. Ball, Water: Water an enduring mystery, *Nature* 452(7185), 291 (2008)
2. P. Gallo, K. Amann-Winkel, C. A. Angell, M. A. Anisimov, F. Caupin, C. Chakravarty, E. Lascaris, T. Loerting, A. Z. Panagiotopoulos, J. Russo, J. A. Sellberg, H. E. Stanley, H. Tanaka, C. Vega, L. Xu, and L. G. M. Pettersson, Water: A tale of two liquids, *Chem. Rev.* 116(13), 7463 (2016)
3. A. Nilsson and L. G. M. Pettersson, The structural origin of anomalous properties of liquid water, *Nat. Commun.* 6, 8998 (2015)
4. H. E. Stanley, Advances in Chemical Physics: Liquid Polymorphism, Vol. 152, John Wiley & Sons, 2013
5. J. H. Simpson and H. Y. Carr, Diffusion and nuclear spin relaxation in water, *Phys. Rev.* 111(5), 1201 (1958)
6. F. Mallamace, C. Corsaro, and H. E. Stanley, A singular thermodynamically consistent temperature at the origin of the anomalous behavior of liquid water, *Sci. Rep.* 2, 993 (2012)
7. F. Mallamace, C. Corsaro, D. Mallamace, C. Vasi, and H. E. Stanley, The thermodynamical response functions and the origin of the anomalous behavior of liquid water, *Faraday Discuss.* 167, 95 (2013)
8. F. Mallamace, C. Corsaro, D. Mallamace, S. Vasi, C. Vasi, and H. E. Stanley, Thermodynamic properties of bulk and confined water, *J. Chem. Phys.* 141(18), 18C504 (2014)
9. H. R. Pruppacher, Self-Diffusion coefficient of supercooled water, *J. Chem. Phys.* 56(1), 101 (1972)
10. NIST Chemistry WebBook, 2008. http://webbook.nist.gov/chemistry/uid/
11. F. Mallamace, C. Corsaro, D. Mallamace, S. Vasi, C. Vasi, H. E. Stanley, and S. H. Chen, Some thermodynamical aspects of protein hydration water, *J. Chem. Phys.* 142(21), 215103 (2015)
12. R. Speedy and C. Angell, Isothermal compressibility of supercooled water and evidence for a thermodynamic singularity at −45°C, *J. Chem. Phys.* 65(3), 851 (1976)
13. P. W. Bridgman, Water, in the liquid and five solid forms, under pressure, in: Proceedings of the American Academy of Arts and Sciences, pp 441–558, JSTOR, 1912
14. G. S. Kell, Density, thermal expansivity, and compressibility of liquid water from 0°C to 150°C: Correlations and tables for atmospheric pressure and saturation reviewed and expressed on 1968 temperature scale, *J. Chem. Eng. Data* 20(1), 97 (1975)
15. G. Kell and E. Whalley, Reanalysis of the density of liquid water in the range 0–150 °C and 0–1 kbar, *J. Chem. Phys.* 62(9), 3496 (1975)
16. C. Sorensen, Densities and partial molar volumes of supercooled aqueous solutions, *J. Chem. Phys.* 79(3), 1455 (1983)
17. D. Hare and C. Sorensen, Densities of supercooled H_2O and D_2O in 25 μ glass capillaries, *J. Chem. Phys.* 84(9), 5085 (1986)
18. D. Hare and C. Sorensen, The density of supercooled water (II): Bulk samples cooled to the homogeneous nucleation limit, *J. Chem. Phys.* 87(8), 4840 (1987)
19. O. Mishima, Volume of supercooled water under pressure and the liquid-liquid critical point, *J. Chem. Phys.* 133(14), 144503 (2010)
20. W. D. Wilson, Speed of sound in distilled water as a function of temperature and pressure, *J. Acoust. Soc. Am.* 31(8), 1067 (1959)
21. R. C. Dougherty and L. N. Howard, Equilibrium structural model of liquid water: Evidence from heat capacity, spectra, density, and other properties, *J. Chem. Phys.* 109(17), 7379 (1998)
22. H. Vogel, The law of the relation between the viscosity of liquids and the temperature, *Phys. Z.* 22, 645 (1921)
23. G. S. Fulcher, Analysis of recent measurements of the viscosity of glasses, *J. Am. Ceram. Soc.* 8(6), 339 (1925)
24. G. Tammann and W. Hesse, The dependence of viscosity upon the temperature of supercooled liquids, *Z. Anorg. Allg. Chem.* 156, 245 (1926)
25. W. S. Price, H. Ide, and Y. Arata, Self-Diffusion of supercooled water to 238 K using PGSE NMR diffusion measurements, *J. Phys. Chem. A* 103(4), 448 (1999)

26. D. Laage and J. T. Hynes, A molecular jump mechanism of water reorientation, *Science* 311(5762), 832 (2006)
27. D. Laage and J. T. Hynes, On the molecular mechanism of water reorientation, *J. Phys. Chem. B* 112(45), 14230 (2008)
28. G. Stirnemann and D. Laage, Direct evidence of angular jumps during water reorientation through two-dimensional infrared anisotropy, *J. Phys. Chem. Lett.* 1(10), 1511 (2010)
29. D. Laage, G. Stirnemann, F. Sterpone, and J. T. Hynes, Water jump reorientation: from theoretical prediction to experimental observation, *Acc. Chem. Res.* 45(1), 53 (2012)
30. D. Laage, G. Stirnemann, F. Sterpone, R. Rey, and J. T. Hynes, Reorientation and allied dynamics in water and aqueous solutions, *Annu. Rev. Phys. Chem.* 62(1), 395 (2011)
31. L. B. Skinner, C. J. Benmore, J. C. Neuefeind, and J. B. Parise, The structure of water around the compressibility minimum, *J. Chem. Phys.* 141(21), 214507 (2014)
32. D. Schlesinger, K. T. Wikfeldt, L. B. Skinner, C. J. Benmore, A. Nilsson, and L. G. M. Pettersson, The temperature dependence of intermediate range oxygen-oxygen correlations in liquid water, *J. Chem. Phys.* 145(8), 084503 (2016)
33. F. Mallamace, C. Corsaro, D. Mallamace, S. Vasi, C. Vasi, and G. Dugo, The role of water in protein's behavior: The two dynamical crossovers studied by NMR and FTIR techniques, *Comput. Struct. Biotechnol. J.* 13, 33 (2015)
34. P. Demontis, J. Gulín-González, M. Masia, M. Sant, and G. B. Suffritti, The interplay between dynamic heterogeneities and structure of bulk liquid water: A molecular dynamics simulation study, *J. Chem. Phys.* 142(24), 244507 (2015)
35. H. W. Horn, W. C. Swope, J. W. Pitera, J. D. Madura, T. J. Dick, G. L. Hura, and T. Head-Gordon, Development of an improved four-site water model for biomolecular simulations: TIP4P-Ew, *J. Chem. Phys.* 120(20), 9665 (2004)
36. P. Demontis, J. Gulín-González, M. Masia, and G. B. Suffritti, The behaviour of water confined in zeolites: molecular dynamics simulations versus experiment, *J. Phys. Condens. Matter* 22(28), 284106 (2010)
37. P. Cicu, P. Demontis, S. Spanu, G. B. Suffritti, and A. Tilocca, Electric-field-dependent empirical potentials for molecules and crystals: A first application to flexible water molecule adsorbed in zeolites, *J. Chem. Phys.* 112(19), 8267 (2000)
38. S. Izadi, R. Anandakrishnan, and A. V. Onufriev, Building water models: A different approach, *J. Phys. Chem. Lett.* 5(21), 3863 (2014)
39. R. Anandakrishnan, C. Baker, S. Izadi, and A. V. Onufriev, Point charges optimally placed to represent the multipole expansion of charge distributions, *PLoS ONE* 8, e67715 (2013)
40. C. Bergonzo and T. E. III Cheatham, Improved force field parameters lead to a better description of RNA structure, *J. Chem. Theory Comput.* 11(9), 3969 (2015)
41. K. Gao, J. Yin, N. M. Henriksen, A. T. Fenley, and M. K. Gilson, Binding enthalpy calculations for a neutral hostguest pair yield widely divergent salt effects across water models, *J. Chem. Theory Comput.* 11(10), 4555 (2015)
42. C. N. Nguyen, T. Kurtzman, and M. K. Gilson, Spatial decomposition of translational water-water correlation entropy in binding pockets, *J. Chem. Theory Comput.* 12(1), 414 (2016)
43. F. Häse and M. Zacharias, Free energy analysis and mechanism of base pair stacking in nicked DNA, *Nucleic Acids Res.* 44 (15), 7100 (2016)
44. A. Mukhopadhyay, I. S. Tolokh, and A. V. Onufriev, Accurate evaluation of charge asymmetry in aqueous solvation, *J. Phys. Chem. B* 119(20), 6092 (2015)
45. J. C. Phillips, R. Braun, W. Wang, J. Gumbart, E. Tajkhorshid, E. Villa, C. Chipot, R. D. Skeel, L. Kale, and K. Schulten, Scalable molecular dynamics with NAMD, *J. Comput. Chem.* 26(16), 1781 (2005)
46. I. C. Yeh and G. Hummer, System-size dependence of diffusion coefficients and viscosities from molecular dynamics simulations with periodic boundary conditions, *J. Phys. Chem. B* 108(40), 15873 (2004)
47. R. G. Gordon, Advances in Magnetic Resonance, Vol. 3, p. 1, New York: Academic Press Inc., 1968
48. A. Y. Zasetsky, Dielectric relaxation in liquid water: Two fractions or two dynamics? *Phys. Rev. Lett.* 107(11), 117601 (2011)
49. C. J. Fecko, J. J. Loparo, S. T. Roberts, and A. Tokmakoff, Local hydrogen bonding dynamics and collective reorganization in water: Ultrafast infrared spectroscopy of HOD/D2O, *J. Chem. Phys.* 122(5), 054506 (2005)
50. J. J. Loparo, S. T. Roberts, and A. Tokmakoff, Multidimensional infrared spectroscopy of water (I): Vibrational dynamics in two-dimensional IR line shapes, *J. Chem. Phys.* 125(19), 194521 (2006)
51. J. J. Loparo, S. T. Roberts, and A. Tokmakoff, Multidimensional infrared spectroscopy of water (II): Hydrogen bond switching dynamics, *J. Chem. Phys.* 125(19), 194522 (2006)
52. J. Stenger, D. Madsen, P. Hamm, E. T. Nibbering, and T. Elsaesser, A photon echo peak shift study of liquid water, *J. Phys. Chem. A* 106(10), 2341 (2002)
53. M. Cowan, B. D. Bruner, N. Huse, J. Dwyer, B. Chugh, E. Nibbering, T. Elsaesser, and R. Miller, Ultrafast memory loss and energy redistribution in the hydrogen bond network of liquid H_2O, *Nature* 434(7030), 199 (2005)
54. A. Luzar and D. Chandler, Hydrogen-bond kinetics in liquid water, *Nature* 379(6560), 55 (1996)

55. A. Luzar and D. Chandler, Effect of environment on hydrogen bond dynamics in liquid water, *Phys. Rev. Lett.* 76(6), 928 (1996)

56. F. W. Starr, J. K. Nielsen, and H. E. Stanley, Fast and slow dynamics of hydrogen bonds in liquid water, *Phys. Rev. Lett.* 82(11), 2294 (1999)

57. F. W. Starr, J. K. Nielsen, and H. E. Stanley, Hydrogen-bond dynamics for the extended simple point-charge model of water, *Phys. Rev. E* 62(1), 579 (2000)

58. A. Luzar, Resolving the hydrogen bond dynamics conundrum, *J. Chem. Phys.* 113(23), 10663 (2000)

59. A. Luzar, Extent of inter-hydrogen bond correlations in water: Temperature effect, *Chem. Phys.* 258(2–3), 267 (2000)

60. V. Voloshin and Y. I. Naberukhin, Hydrogen bond lifetime distributions in computer simulated water, *J. Struct. Chem.* 50(1), 78 (2009)

61. H. Martiniano and N. Galamba, Insights on hydrogen-bond lifetimes in liquid and supercooled water, *J. Phys. Chem. B* 117(50), 16188 (2013)

62. B. Mukherjee, Microscopic origin of temporal heterogeneities in translational dynamics of liquid water, *J. Chem. Phys.* 143(5), 054503 (2015)

63. O. Conde and J. Teixeira, Hydrogen bond dynamics in water studied by depolarized Rayleigh scattering, *J. Phys.* 44(4), 525 (1983)

64. J. Teixeira, M. C. Bellissent-Funel, S. H. Chen, and A. J. Dianoux, Experimental determination of the nature of diffusive motions of water molecules at low temperatures, *Phys. Rev. A* 31(3), 1913 (1985)

65. C. Fecko, J. Eaves, J. Loparo, A. Tokmakoff, and P. Geissler, Ultrafast hydrogen-bond dynamics in the infrared spectroscopy of water, *Science* 301(5640), 1698 (2003)

66. D. Laage, Reinterpretation of the liquid water quasi-elastic neutron scattering spectra based on a nondiffusive jump reorientation mechanism, *J. Phys. Chem. B* 113(9), 2684 (2009)

67. R. Kumar, J. Schmidt, and J. Skinner, Hydrogen bonding definitions and dynamics in liquid water, *J. Chem. Phys.* 126(20), 204107 (2007)

68. D. Prada-Gracia, R. Shevchuk, and F. Rao, The quest for self-consistency in hydrogen bond definitions, *J. Chem. Phys.* 139(8), 084501 (2013)

69. A. Ozkanlar, T. Zhou, and A. E. Clark, Towards a unified description of the hydrogen bond network of liquid water: A dynamics based approach, *J. Chem. Phys.* 141(21), 214107 (2014)

70. P. Wernet, D. Nordlund, U. Bergmann, M. Cavalleri, M. Odelius, H. Ogasawara, L. Å. Näslund, T. K. Hirsch, L. Ojamäe, P. Glatzel, L. G. M. Pettersson, and A. Nilsson, The structure of the first coordination shell in liquid water, *Science* 304(5673), 995 (2004)

71. R. H. Henchman and S. J. Irudayam, Topological hydrogen-bond definition to characterize the structure and dynamics of liquid water, *J. Phys. Chem. B* 114(50), 16792 (2010)

72. J. Jonas, T. DeFries, and D. Wilbur, Molecular motions in compressed liquid water, *J. Chem. Phys.* 65(2), 582 (1976)

73. J. Ropp, C. Lawrence, T. Farrar, and J. Skinner, Rotational motion in liquid water is anisotropic: a nuclear magnetic resonance and molecular dynamics simulation study, *J. Am. Chem. Soc.* 123(33), 8047 (2001)

74. E. H. Hardy, A. Zygar, M. D. Zeidler, M. Holz, and F. D. Sacher, Isotope effect on the translational and rotational motion in liquid water and ammonia, *J. Chem. Phys.* 114(7), 3174 (2001)

75. R. Ludwig, F. Weinhold, and T. C. Farrar, Experimental and theoretical determination of the temperature dependence of deuteron and oxygen quadrupole coupling constants of liquid water, *J. Chem. Phys.* 103(16), 6941 (1995)

76. J. A. Sellberg, C. Huang, T. A. McQueen, N. D. Loh, H. Laksmono, et al., Ultrafast X-ray probing of water structure below the homogeneous ice nucleation temperature, *Nature* 510(7505), 381 (2014)

77. C. Angell and F. Franks, Water: A Comprehensive Treatise, Vol. 7, New York: Plenum, 1982

78. H. E. Stanley and O. Mishima, The relationship between liquid, supercooled and glassy water, *Nature* 396(6709), 329 (1998)

79. L. Liu, S. H. Chen, A. Faraone, C. W. Yen, and C. Y. Mou, Pressure dependence of fragile-to-strong transition and a possible second critical point in supercooled confined water, *Phys. Rev. Lett.* 95(11), 117802 (2005)

80. S. V. Lishchuk, N. P. Malomuzh, and P. V. Makhlaichuk, Why thermodynamic properties of normal and heavy water are similar to those of argon-like liquids? *Phys. Lett. A* 374(19–20), 2084 (2010)

81. A. Fisenko, N. Malomuzh, and A. Oleynik, To what extent are thermodynamic properties of water argon-like? *Chem. Phys. Lett.* 450(4–6), 297 (2008)

82. S. Izadi, B. Aguilar, and A. V. Onufriev, Proteinligand electrostatic binding free energies from explicit and implicit solvation, *J. Chem. Theory Comput.* 11(9), 4450 (2015)

83. D. Nayar and C. Chakravarty, Sensitivity of local hydration behaviour and conformational preferences of peptides to choice of water model, *Phys. Chem. Chem. Phys.* 16(21), 10199 (2014)

84. R. B. Best and J. Mittal, Protein simulations with an optimized water model: Cooperative helix formation and temperature-induced unfolded state collapse, *J. Phys. Chem. B* 114(46), 14916 (2010)

85. R. B. Best and J. Mittal, Free-energy landscape of the gb1 hairpin in all-atom explicit solvent simulations with different force fields: Similarities and differences, *Proteins* 79(4), 1318 (2011)

86. P. Florová, P. Sklenovský, P. Banáš, and M. Otyepka, Explicit water models affect the specific solvation and dynamics of unfolded peptides while the conformational behavior and flexibility of folded peptides remain intact, *J. Chem. Theory Comput.* 6(11), 3569 (2010)
87. H. E. Stanley, S. V. Buldyrev, G. Franzese, N. Giovambattista, and F. W. Starr, Static and dynamic heterogeneities in water, *Philosophical Transactions of the Royal Society of London A* 363(1827), 509 (2005)
88. A. Nilsson and L. Pettersson, Perspective on the structure of liquid water, *Chem. Phys.* 389(1–3), 1 (2011)
89. D. Prada-Gracia, R. Shevchuk, P. Hamm, and F. Rao, Towards a microscopic description of the free-energy landscape of water, *J. Chem. Phys.* 137(14), 144504 (2012)
90. G. C. Picasso, D. C. Malaspina, M. A. Carignano, and I. Szleifer, Cooperative dynamic and diffusion behavior above and below the dynamical crossover of supercooled water, *J. Chem. Phys.* 139(4), 044509 (2013)
91. J. A. Sellberg, S. Kaya, V. H. Segtnan, C. Chen, T. Tyliszczak, H. Ogasawara, D. Nordlund, L. G. M. Pettersson, and A. Nilsson, Comparison of X-ray absorption spectra between water and ice: New ice data with low pre-edge absorption cross-section, *J. Chem. Phys.* 141(3), 034507 (2014)
92. E. Duboué-Dijon and D. Laage, Characterization of the local structure in liquid water by various order parameters, *J. Phys. Chem. B* 119(26), 8406 (2015)
93. R. S. Singh, J. W. Biddle, P. G. Debenedetti, and M. A. Anisimov, Two-state thermodynamics and the possibility of a liquid-liquid phase transition in supercooled TIP4P/2005 water, *J. Chem. Phys.* 144(14), 144504 (2016)
94. Y. Xu, N. G. Petrik, R. S. Smith, B. D. Kay, and G. A. Kimmel, Growth rate of crystalline ice and the diffusivity of supercooled water from 126 to 262 K, *Proc. Natl. Acad. Sci. USA* 113(52), 14921 (2016)
95. K. A. Jackson, Kinetic Processes: Crystal Growth, Diffusion, and Phase Transitions in Materials, Wiley-VCH Verlag GmbH & Co. KGaA, 2005
96. W. L. Jorgensen, J. Chandrasekhar, J. D. Madura, R. W. Impey, and M. L. Klein, Comparison of simple potential functions for simulating liquid water, *J. Chem. Phys.* 79(2), 926 (1983)
97. J. L. F. Abascal and C. Vega, A general purpose model for the condensed phases of water: TIP4P/2005, *J. Chem. Phys.* 123(23), 234505 (2005)
98. M. D. Marzio, G. Camisasca, M. Rovere, and P. Gallo, Fragile-to-strong crossover in supercooled water: A comparison between TIP4P and TIP4P/2005 models, *Nuovo Cim.* 39(C), 302 (2016)